RSC Advances

A facile one-pot synthesis of three-dimensional microflower birnessite (δ-MnO2) and its efficient oxidative degradation of Rhodamine B

Journal:	*RSC Advances*
Manuscript ID	RA-ART-11-2015-024848.R1
Article Type:	Paper
Date Submitted by the Author:	30-Jan-2016
Complete List of Authors:	Qin, Minggao; College of Chemistry and Chemical Engineering, Hunan University, Changsha, P.R.China Zhao, Haoliang; College of Chemistry and Chemical Engineering, Hunan University, Changsha, P.R.China Yang, Weijun; Hunan University, College of Chemistry and Chemical Engineering Zhou, Yuanrong; College of Chemistry and Chemical Engineering, Hunan University, Changsha, P.R.China Li, Feng; College of Chemistry and Chemical Engineering, Hunan University, Changsha, P.R.China
Subject area & keyword:	Nanoscience - Environmental < Environmental

SCHOLARONE™
Manuscripts

A facile one-pot synthesis of three-dimensional microflower birnessite (δ-MnO$_2$) and its efficient oxidative degradation of Rhodamine B

Minggao Qin, Haoliang Zhao, Weijun Yang*, Yuanrong Zhou, Feng Li

Abstract: High purity of birnessite (δ-MnO$_2$) was obtained by a facile one-pot method using MnSO$_4$·H$_2$O as Mn resource, ethylenediamine tetraacetic acid disodium salt (EDTA-Na) as complexing agent and oxygen in air as oxidant under alkaline condition. The as-prepared birnessite presented three-dimensional microflower composed of two-dimensional ultrathin nanosheets. The degradation results indicated that the prepared δ-MnO$_2$ possessed excellent removal of Rhodamine B (RhB). Typically, 50 ml of RhB (10 mg/L) could be degraded completely with 10 mg sample in 5 min without any additives such as hydrogen peroxide, peroxysulphate or any supplementary means such as microwave, ultrasound. The samples were characterized by Fourier transform infrared spectroscopy (FTIR), X-ray diffraction (XRD), X-ray photoelectron spectroscopy (XPS), field emission scanning electron microscopy (FESEM), N$_2$ gas adsorption–desorption and thermogravimetry analysis (TGA) techniques. The mechanism of the degradation process was proposed and discussed that a redox reaction between birnessite and RhB occurred under acidic environment. Clearly, the as-prepared birnessite provides a great potential for rapid degradation of dyes and organic pollutants. As its starting materials easily available, simple method to be synthesized and undemanding degradation conditions, the as-prepared birnessite has high practical value in treating environmental pollutants.

Keywords: Birnessite; Morphology control; Oxidation degradation; Rhodamine B

1. Introduction

During the past decades, manganese dioxides (MnO$_2$) are an important and well-studied class of materials in various domains due to their outstanding structural flexibility combined with novel chemical and physical properties.[1] MnO$_2$ has many kinds of polymorphs, such as α, β, γ and δ-MnO$_2$. The crystal structures are convinced to be responsible for their properties, and the controlled preparation of MnO$_2$ has drawn interests of scientific researchers.[2] Among them, especially, δ-MnO$_2$ birnessite has attracted extensive attention for its distinctive layered structure which contain two-dimensional sheets of edge-sharing MnO$_6$ octahedra. The sheets with a basal spacing of about 0.7 nm are supported by basic mental ions (Li$^+$, Na$^+$, K$^+$) and water molecules.[3] These cations balance the negative charge arising from the layers as a consequence of the presence of Mn ions with an oxidation number lower than +4.[4] Moreover, the existence of mixed valencies (mainly +4, +3, or +2) are very important in electron transport during the chemical reactions.[5]

Due to its unique chemicophysical properties mentioned above, birnessites have been widely applied: elimination of organic pollutants,[6-8] supercapacitor[9, 10] and electrode material[11, 12] and so forth. At present, birnessites were mainly synthesized by reduction of $KMnO_4$ with organic substances following sol-gel method;[13, 14] decomposition of $KMnO_4$ under acid condition at a water boiling temperature;[4, 15] and oxidation of Mn^{2+} solution bubbled with oxygen or hydrogen peroxide[16] in alkali media. Although, the reduction method is easy to control the morphology of products, it's time and energy consuming which usually needs post-treatment under high temperature for a relative long time. For the latter method, it is difficult to obtain pure birnessite because of a side reaction in an alkali medium, in which hausmannite is easy produced.[17]

Among the applications of birnessite stated above, the degradation of dyes is one of the hottest topics, because organic dye pollutants in water have become a major source of environmental pollution for its structure stability and resistance to degradation.[18] More seriously, the residual dyes create severe problems to the ecosystem and even human health.[8] Therefore, it is very essential and urgent to solve this austere problem. So far, numerous studies have reported to deal with dye wastewaters including physical and chemical processes. For examples, adsorption on activated carbon[19], photocatalytic degradation,[20, 21] oxidation by adding oxygenants such as H_2O_2[22], persulfate[18] and even with the assistance of microwave [23] or ultrasonic [24]. However, these methods suffer from sophisticated and strict conditions, which restrain their commercial applications.

In this research, a facile one-pot method to synthesize high purity of birnessite was reported. RhB (the molecular model shown in Scheme. 1) was chosen as the representative organic dye due to its low degradability by the conventional methods[8]. The as-prepared birnessite possessed a high oxidation degradation performance to RhB, which could be degraded completely in a short time without adding any additives or using supplementary means. The main influence factors during the preparation and degradation were discussed seriously, and also the degradation mechanism.

Scheme. 1 Molecular model of Rhodamine B

2. Experimental

2.1 Chemical and materials

The commercially available dye Rhodamine B was purchased from Shanghai Chemical Reagent Company, China. All the other chemicals $MnSO_4 \cdot H_2O$, EDTA-Na, NaOH and H_2SO_4 were of analytical grade and provided from Tianjin, China. They were used as received without further purifications.

2.2 Preparation of birnessite

In this article, birnessite was prepared through a facile one-pot method which avoided post-treatment and side reactions. A typical procedure of synthesizing

birnessite is as follows: equimolar amount (8 mmol) of $MnSO_4 \cdot H_2O$ and EDTA-Na were dissolved in 25 mL deionized water, then a solution of 50 mL 1.2 mol/L NaOH was dropped to the former solution slowly with a speed of 3 mL/min. The color of the solution changed affluently during the process, and black precipitate emerged eventually. The final suspension stirred continuously for another one hour. Every step mentioned above was accompanied by a constant magnetic stirring to make the additives dissolve and react completely. The yielded solid product was filtered, washed with distilled water several times to remove any possible residual reactants. Finally, the product was dried in air at 50 °C overnight. In order to explore the effect of EDTA-Na on the formation of birnessite, a similar experiment was conducted without adding EDTA-Na at the beginning, while other parameters kept the same.

2.3 Characterization of birnessite

Synthesized products were identified by X-ray diffraction (XRD) at room temperature using a Shimadzu 6100 instrument with Cu Kα radiation operated at 40 kV and 30 mA. Fourier transform infrared spectroscopy (FTIR, Shimadzu 8400S) was carried out by making pellets with KBr powder. Scanning electron microscopy (SEM) investigations were carried out on a JEOL JEM 6700 field-emission scanning electron microscope. The specific surface area of the product was determined by multipoint N_2-BET analysis using a Coulter (SA 3100) surface area analyzer. X-ray photoelectron spectroscopy (XPS) spectra were obtained using a PHI Quantera SXM (PHI-5300/ESCA, ULVAC-PHI, INC). An Al Kα X-ray beam was used with a power of 250 W. The base vacuum of the chamber was maintained at 3×10^{-9} torr during XPS analysis. Prior to the measurement, the electrode was washed with water to remove electrolyte.

2.4 Oxidative degradation of RhB

The degradation of RhB was carried out in a glass beaker (200 ml) under magnetic stirring. 10 mg of birnessite was added to the beaker containing 50 mL deionized water. After ultrasonication treatment for 5 min, RhB dye (1 mL, 500 mg/L) was injected to above solution and the mixture was continuously stirred for 30 min, to ensure that a suitable adsorption/desorption equilibrium of the dye on the sample surface had been established. After that, diluted H_2SO_4 solution (0.8 M) was used to adjust the pH of final RhB solution.

At given intervals, appropriate amount of suspension was taken out and filtered to remove the solid particles before analysis. The concentration of RhB was measured by a Labtech UV BuleStar Plus spectrophotometer set at an absorbance maximum of 554 nm. The degradation rate R of RhB was calculated by Eq. (1):

$$R = (C_0 - C_t)/C_0 \times 100\% \quad (1)$$

Where, C_0 (mg/L) and C_t (mg/L) are the initial and final RhB, respectively. It is used to evaluate the activity of birnessite.

3. Results and discussion

3.1. Characterizations of the synthetic products

XRD analysis was used to determine the crystal structure of the samples. Fig. 1 (a) showed XRD pattern of the typical sample obtained in the existence of EDTA-Na. All the peaks in the pattern are perfectly indexed to birnessite ($Na_{0.55}MnO_2 \cdot 1.5H_2O$: JCPDF 43-1456). No peaks of other phases were emerged, indicating the high purity of the product. The strong and sharp reflection peaks suggest that the as-prepared birnessite was well crystallized. By comparison, the pure hausmannite (Mn_3O_4: JCPDF 01-1127) was obtained without adding EDTA-Na in the initial $MnSO_4$ solution, as shown in Fig. 1 (b).

Notably, the existence of EDTA-Na or not had an evident effect on the kinds of products. When adding EDTA-Na to $MnSO_4 \cdot H_2O$, the Mn^{2+} in the solution would complex with EDTA-Na, resulting in the decrease of Mn^{2+} concentration, and the Mn^{2+} would be released step by step with the consuming of Mn^{2+} when dropping NaOH solution, so that as soon as the $Mn(OH)_2$ produced, it could be immediately and adequately oxidized to Mn^{4+} by the atmospheric oxygen. The proposed process can be explained by two reactions (2), (3) as follows:

$$Mn^{2+}+2OH^- =Mn(OH)_2 \qquad (2)$$
$$Mn(OH)_2+1/2O_2=MnO_2+H_2O \qquad (3)$$
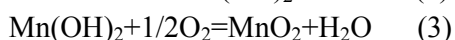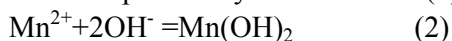
In this paper, only the preparation and the degradation performance of birnessite will be discussed, and the hausmannite will not be mentioned temporary.

Fig.1. XRD pattern of the synthesized products: (a) with EDTA-Na, (b) without EDTA-Na.

Then, the influence of the concentration of EDTA-Na on the products was examined. The XRD patterns (not shown) suggested the products were birnessites whatever the molar ratio of $MnSO_4$/EDTA-Na equals to 1: 1 or 2: 1. The morphology and structure of birnessite products were investigated by FESEM. The FESEM images of birnessites prepared under different conditions were shown in Fig. 2. When the molar ratio of $MnSO_4$/EDTA-Na equals to 1: 1, apparently, the as-synthesized birnessite consist of spherical particles, with sizes about 5 μm (Fig. 2a). While at a higher magnification, it is obvious that the spherical particles present three-dimensional mircoflower structure, which composed of ultrathin two-dimensional nanosheets with less than one hundred nanometers (Fig. 2b).When the ratio $MnSO_4$/EDTA-Na came to 2: 1, the morphology and structure were different. It can be clearly seen that some birnessite particles aggregated together and no clear edges between them Fig.2 (c), and irregular porous structure was observed due to the ruleless arrangement of sheets shown in Fig.2 (d). It can be concluded that the concentration of EDTA-Na greatly influenced on the morphology of the birnessite, and it is likely that the EDTA-Na also serve as a structure-directing agent in this process. Thus in this way, the morphology of the products can be controlled through adjusting the concentration of EDTA-Na.

Fig. 2 Typical SEM images of birnessites prepared under the molar ratio of MnSO4/EDTA-Na equals to 1 (a), (b) and the ratio equals to 2 (c), (d). The lower-magnification image are shown in (a), (c), while the higher-magnification images are presented in (b), (d).

Metal-oxygen bonds are sensitive to infrared, and hence disordered components can be elucidated by infrared analysis. Taking mircoflower sample as example, the FTIR spectrum further confirmed the formation of birnessite. As shown in Fig. 3, FTIR spectrum presents that a broad, medium band centered around 3370 cm^{-1} due to OH- antisymmetric stretching vibration of associated (hydrogen-bonded) hydroxyl groups, [25] while the band at 1630 cm^{-1} is due to the bending vibrations of O-H groups of the adsorbed water molecules.[26] In the Far-IR range, birnessite exhibits three IR bands located at 514, 477, and 415 cm^{-1} (insert in Fig. 3) were consistent with the previous report.[27] In which the two peaks at 514 and 477 cm^{-1} correspond to Mn-O stretching vibrations and are characteristic IR bands in birnessite,[28, 29] and it is worth noting that the peak emerged at 514 cm^{-1} is due to the MnO_6 octahedral structure.[30]

Fig. 3. FTIR spectra of birnessite, the inset shows partially enlarged spectra in the range of 700–400 cm^{-1}.

Similarly, TG and DTA curves of mircoflower birnessite were shown in Fig. 4, which consists of four steps obviously: firstly, a weight loss of about 10.8 wt.% corresponds to evaporation of (surface) adsorbed water of birnessite from room temperature to 150 °C;[31] Secondly, the weight loss of 5.8 wt % is ascribed to the dehydration of the crystal water existing in the interlayers of birnessite in the temperature range of 250−350 °C;[32] Then, the significant weight loss between 500 and 600 °C can be assigned to oxygen release, resulting in the phase transformation from MnO_2 to Mn_2O_3; And last, above 650 °C is mainly due to the transformation from Mn_2O_3 to Mn_3O_4 accompanied by further oxygen release.[33]

Figure 4. TG-DTA curves of birnessite in N_2. Heating rate: 10 °C/min.

3.2 Oxidative degradation of RhB by birnessite

The oxidative degradation experiment was conducted at ambient temperature without adding any oxidants or utilizing supplementary devices. The solution pH was proved to be the main influencing factor on oxidative degradation of RhB.

Fig. 5 showed the changes of UV-vis spectra of RhB during degradation under different pH (pH=7, 5, 3 and 1). When the degradation progress was conducted in neutral solution, the UV-vis spectra only presented a slightly decrease in λ_{max}=554 nm due to the adsorption of RhB on birnessite, as it showed in Fig. 5 (a). Moreover，the adsorption-desorption equilibrium of RhB on the surface of birnessite was reached in 20 min. While adjusting the pH to 5 (Fig.5 (b)) by using diluted H_2SO_4, the maximum adsorption peak shifted from 554 to 498 nm which was caused by the N-deethylation of RhB resulted in Rh.[34] With the time increasing, the intensity of λ_{max} almost kept unchanged, which indicated that deethylation dominated in this degradation condition. Fig. 5 (c) showed the UV-vis spectra under pH=3. By contrast to Fig. 5 (b), there existed an evident decrease in 498 and 254 nm, which demonstrated the cleavage of the whole chromophore structure (cycloreversion) of RhB.[35] The same tendency was observed, as shown in Fig. 5 (d), obviously, less time was needed to reach the same degradation rate under pH=1. These results presented above implied that the degradation reaction only occurred under acid condition, and the lower the pH the

faster the degradation rate. The detail degradation rates were presented in Fig. 5 (e), the absorption capacity were negligible (less than 3%) in diverse pH values. At pH =1, the degradation rate reached 95% in 3 min, and almost 100% after 5 min, which showed a very efficient degradation rate. This result were distinctively excellent compared to the previous reports.[24, 34, 36, 37]

At the mean time,two blank experiments were conducted without birnessite under pH=1, and the pH was adjusted by dropping H_2SO_4 or HCl. When the reaction was conducted in the absence of the birnessite, the concentration of RhB almost kept the same, indicating the birnessite was indispensable for the degradation of RhB. And whichever kind of acid was used, the results showed almost the same as long as the pH of the solution was adjusted to the same.

In fact, the suspension pH exerted two double-edged effects on RhB degradation. At lower pH, one hand, the crystal stability of the layered structure of birnessite is weak,[21] which is beneficial to the redox reaction between $Mn^{4+/3+}$ and RhB; meanwhile, high H^+ concentration could improve reducing potential of the system according to the Nernst Equation,[38] that is to say, a decrease in suspension pH would increase oxidizing power of the system. On the other hand, the strong acidity would restrain the absorption of RhB on the surface of birnessite, which would affect the reaction rate between RhB and birnessite. According to the results, it can be concluded that the pH play a crucial role on degrading RhB, and influence of the absorption of RhB on birnessite is negligible for its low absorption capacity.

Fig. 5. The UV-vis spectra of RhB during degradation under different pH: (a) pH=7; (b) pH=5; (c) pH=3; (d) pH=1. (e) Detailed degradation rates under different pH values.

In order to figure out the degradation mechanism of birnessite, the influences of oxygen and sunlight were also investigated. One experiment was conducted without oxygen, the oxygen in the solution and sample were eliminated before using, and the degradation reaction was protected in the N_2 atmosphere. Another was done in the dark. The results were shown in Fig.6, it can be clearly seen that the two factors had limited effect on the degradation processes.

In the anaerobic or dark experiments, the degradation of RhB on birnessite resulted from the effect of adsorption and oxidation of birnessite under acid condition. As represented above, the adsorption of RhB on birnessite is ignorable. According to the report,[39] the release of lattice oxygen would occur only at a high temperature exceed 140 °C, that is to say, it is impossible to release lattice oxygen at the room temperature in this study. The conclusion was also consistent with the TG results. So the RhB degradation reaction is caused by reduction of Mn^{4+}, which indicates the oxidation of birnessite was the main mechanism for RhB degradation.

Fig. 6. The degradation rates of RhB under different experimental conditions

To elucidate the relationship between the structure and performance of birnessite, the specific surface area and porosity were measured by N_2 adsorption measurements, shown in Fig. 7. The pore volume and specific surface areas (S_{BET}) was only 0.178 cm^3/g and 19.7 m^2/g respectively which were much smaller than the previous reports.

[40, 41] The pore size distribution was mainly in the range of 10-50 nm, and the average pore diameter is about 30.8 nm. Even though the S_{BET} of the material is very important and even determines its physical or chemical performances,[42] the small S_{BET} of as prepared birnessite showed an efficient oxidative degradation of RhB indicated that the S_{BET} of birnessite was not critical for this oxidative degradation progress. Moreover, the small S_{BET} could also be used to demonstrate the phenomenon why only a slight decrease in intensity of RhB after adsorption-desorption equilibrium.

Fig. 7. N_2 adsorption–desorption isotherms of birnessite

XPS is a well-established surface analysis technique. XPS spectra can be used to determine the oxidation states of constituents at mineral surfaces. Here, XPS was used to further demonstrate the degradation reaction occurred between birnessite and RhB. For both fresh and used birnessites, two peaks at 654.0 and 642.0 eV showed in Fig.6 (a), which correspond to the binding energy of Mn $2p_{1/2}$ and Mn $2p_{3/2}$ respectively.[43] Note that the Mn $2p_{3/2}$ binding energy of used birnessite was slightly shifted from 642 to 641.8 eV in comparison with that of fresh birnessite as shown in insert of Fig.8 (a).

In order to figure out the changes of the oxidation states of manganese which is attributed to demonstrate the reaction mechanism, the relative abundance of Mn^{4+}, Mn^{3+} and Mn^{2+} species for each sample was obtained by studying the $Mn2p_{3/2}$ spectra. The spectra of fresh birnessite was decomposed into three components corresponding to Mn^{4+} (642.9 eV), Mn^{3+} (642.0 eV) and Mn^{2+} (640.9 eV) species.[44] While for the used birnessite, no obvious peak was immerged at about 640.9 eV, indicating the trace amount of Mn^{2+}. This was the results of Mn^{2+} released into the solution under acid condition, it was worth noting that the Mn^{2+} contained two parts: one was the original existence Mn^{2+} in the sample, the other was arising from reductive dissolution of Mn^{4+} with RhB as electron donor.

Using multiplet fitting of the $Mn2p_{3/2}$ peaks, the contents of Mn^{4+}, Mn^{3+} and Mn^{2+} on the surface of fresh birnessite were about 44.9 %, 40.4 % and 14.7 % respectively, and Mn^{4+}, Mn^{3+} were 41.4% and 58.6 % for used birnessite. The decline of the relative contents of Mn^{4+}/Mn^{3+} due to the reduction of Mn^{4+} to Mn^{3+} and Mn^{2+}. For comparison, the Fig. 8 (d) showed the XPS $Mn2p_{3/2}$ spectrum of birnessite treated in solution pH=1 without RhB, which showed a similar spectrum to used birnessite and the relative contents of Mn^{4+} and Mn^{3+} were 48.3 % and 51.7 %, the ratio of Mn^{4+}/Mn^{3+} was lower than that of fresh birnessite while higher than used birnessite. This results indicated that Mn^{4+} was more inclined to be reduced with the existence of RhB.

Fig. 8. XPS spectra of fresh birnessite, used birnessite and birnessite treated in acid solution without RhB: (a) Mn2p, insert was the Mn2p XPS around 642 eV. Mn ($2p_{3/2}$) for those samples respectively: (b), (c) and (d).

Unlike common catalysts, the as-prepared birnessite severed as an oxidant during the degradation, which meant it would be consumed gradually. The efficiency of RhB degradation in a successive batch system was shown in Fig.9 (a). For the first four rounds, the loss of activities were not noticeable, and all the degradation rates kept

around 98% in 5 min. While from the fifth round, more time were needed to reach a similar degradation rates, and the maximum degradation rate decreased to 72% even over 70 min when it came to the eighth round. The result was understandable for the reduction of birnessite and inescapable absorption of degradation products on the surface of birnessite. Besides the decrease of peak intensity, the XRD patterns of the sample still retained unchanged after degradation reaction of RhB several circles, as shown in Fig. 9 (b), indicating that the unchanged structure of birnessite.

4. Conclusion

In this paper, three-dimensional microflower composed of two-dimensional ultrathin nanosheets birnessite was synthesized by using a facile one-pot method. The use of EDTA-Na played a critical role on the product and its morphology and structure, which can be controlled by adjusting the molar ratio of $MnSO_4$/EDTA-Na. EDTA-Na is not only a complexing agent but also severs as a structure-directing agent. The as-prepared microflower birnessite was used to degrade the RhB. 50 ml of RhB (10 mg/L) could be degraded completely with 10 mg sample in 5 min without adding any oxidizers   such as H_2O_2 and peroxysulphate or utilizing supplementary means such as microwave and ultrasound. The solution pH had a great effect on the degradation rates, the lower the pH, the faster the degradation speed. While the influence of absorption capacity of birnessite was negligible for its small specific surface area. The degradation mechanism was investigated, a redox reaction was occurred between RhB and birnessite under acid condition. When solution pH=5, only deethylation reaction happened，while deethylation and cycloreversion occurred simultaneously at lower pH (1-3). Due to its starting materials easily available, simple method to be synthesized and undemanding degradation conditions, the as-prepared birnessite possesses high practical value in treating environmental pollutants.

Acknowledgment

References

1 S. L. Suib, *Acc. Chem. Res.*, 2008, **41**, 479-487.

2 G. Cheng, L. Yu, T. Lin, R. Yang, M. Sun, B. Lan, L. Yang and F. Deng, *J. Solid State Chem.*, 2014, **217**, 57-63.

3 F. Shiraishi, S. Ikeda and N. Kamikariya, *Chem. Eng. J.*, 2009, **148**, 234-241.

4 P. Di Leo, M. D. Pizzigallo, V. Ancona, F. Di Benedetto, E. Mesto, E. Schingaro and G. Ventruti, J. Hazard. Mater., 2012, **201-202**, 148-154.

5 X. Chen, Y. F. Shen, S. L. Suib and C. L. O'Young, *Chem. Mater.*, 2002, **14**, 940-948.

6 J. Wang, P. Zhang, J. Li, C. Jiang, R. Yunus and J. Kim, *Environ. Sci. Technol.*, 2015, **49**, 12372-12379.

7 A. Kamimura, Y. Nozaki, S. Ishikawa, R. Inoue and M. Nakayama, *Tetrahedron Lett.*, 2011, **52**, 538-540.

8 S. Kaur, V. Bhalla and M. Kumar, *ACS Appl. Mater. & Inter.*, 2015, **7**, 16617-16624.

9 D. Yan, H. Zhang, S. Li, G. Zhu, Z. Wang, H. Xu and A. Yu, *J. Alloy. Compd.*, 2014, **607**, 245-250.

10 S. Zhao, T. Liu, D. Hou, W. Zeng, B. Miao, S. Hussain, X. Peng and M. S. Javed, *Appl. Surf. Sci.*, 2015, **356**, 259-265.

11 M. H. Alfaruqi, J. Gim, S. Kim, J. Song, D. T. Pham, J. Jo, Z. Xiu, V. Mathew and J. Kim, *Electrochem.Commun.*, 2015, **60**, 121-125.

12 L. Dang, C. Wei, H. Ma, Q. Lu and F. Gao, *Nanoscale*, 2015, **7**, 8101-8109.

13 M. Ghaly, F. M. S. E. El-Dars, M. M. Hegazy and R. O. Abdel Rahman, *Chem. Eng. J.*, 2015, **284**, 1373-1385

14 H. M. Chen and J. H. He, *J Phys Chem C*, 2008, **112**, 17540-17545.

15 M. D. Pizzigallo, P. D. Leo, V. Ancona, M. Spagnuolo and E. Schingaro, *Chemosphere*, 2011, **82**, 627-634.

16 E. Eren, M. Guney, B. Eren and H. Gumus, *Appl. Catal. B: Environ.*, 2013, **132-133**, 370-378.

17 F. X. Han, Z. Y. Qun, T. W. Fen and L. Fan, *Pedosphere*,2004,**14**,63-70.

18 S. Su, W. Guo, Y. Leng, C. Yi and Z. Ma, *J. Hazard. Mater.*, 2013, **244-245**, 736-742.

19 Y. Aldegs, M. Elbarghouthi, A. Elsheikh and G. Walker, *Dyes Pigments*, 2008, **77**, 16-23.

20 L. Zhang, W. Wang, L. Zhou and H. Xu, *Small*, 2007, **3**, 1618-1625.

21 H. J. Cui, H. Z. Huang, B. Yuan and M. L. Fu, *Geochem. T.*, 2015, **16**, 10.

22 X. Peng and I. Ichinose, *Nanotechnology*, 2011, **22**, 015701-015707.

23 L. Li, X. Zhang, W. Zhang, L. Wang, X. Chen and Y. Gao, *Colloid Surf. A-Physicochem. Eng. Asp.*, 2014, **457**, 134-141.

24 M. Zhou, H. Yang, T. Xian, R. S. Li, H. M. Zhang and X. X. Wang, *J. Hazard. Mater.*, 2015, **289**, 149-157.

25 F. A. Al-Sagheer and M. I. Zaki, *Micropor. Mesopor. Mat.*, 2004, **67**, 43-52.

26 C. Xia, G. Lv, L. Mei, K. Song, Z. Li, X. Wang, X. Xing and B. Xu, *Water Air & Soil Poll.*, 2014, **225**.

27 A. Iyer, J. Del-Pilar, C. K. King'ondu, E. Kissel, H. F. Garces, H. Huang, A. M. El-Sawy, P. K. Dutta and S. L. Suib, *J. Phys.Chem. C*, 2012, **116**, 6474-6483.

28 N.-H. Wang and S.-L. Lo, *Appl. Surf. Sci.*, 2014, **299**, 123-130.

29 D. Yan, P. X. Yan, S. Cheng, J. T. Chen, R. F. Zhuo, J. J. Feng and G. A. Zhang, *Cryst. Growth & Des.*, 2009, **9**, 218-222.

30 Y. Xin Zhang, X. Long Guo, M. Huang, X. Dong Hao, Y. Yuan and C. Hua, *J.Phys. Chem. Solids*, 2015, **83**, 40-46.

31 A. Napola, M. D. Pizzigallo, P. Di Leo, M. Spagnuolo and P. Ruggiero, *Chemosphere*, 2006, **65**, 1583-1590.

32 J. F. Wang, G. N. Zhang, L. J. Ren, L. P. Kang, Z. P. Hao, Z. B. Lei and Z. H. Liu, *Cryst. Growth & Des.*, 2014, **14**, 5626-5633.

33 F. Schurz, J. M. Bauchert, T. Merker, T. Schleid, H. Hasse and R. Gläser, *Appl.Catal. A: Gen.*, 2009, **355**, 42-49.

34 J. Zhuang, W. Dai, Q. Tian, Z. Li, L. Xie, J. Wang, P. Liu, X. Shi and D. Wang, *Langmuir*, 2010, **26**, 9686-9694.

35 N. Daneshvar, M. A. Behnajady, M. K. A. Mohammadi and M. S. S. Dorraji, *Desalination*, 2008, **230**, 16-26.

36 A. Umar, M. S. Akhtar, G. N. Dar and S. Baskoutas, *Talanta*, 2013, **116**, 1060-1066.

37 L. Zhu, Z. D. Meng, C. Y. Park, T. Ghosh and W. C. Oh, *Ultrason. Sonochem.*, 2013, **20**, 478-484.

38 M. X. Zhu, Z. Wang and L. Y. Zhou, *J. Hazard. Mater.*, 2008, **150**, 37-45.

39 J. Luo, Q. Zhang, J. Garcia-Martinez and S. L. Suib, *J. Am. Chem. Soc.*, 2008, **130**, 3198-3207.

40 C. Chen, G. Ding, D. Zhang, Z. Jiao, M. Wu, C. H. Shek, C. M. Wu, J. K. Lai and Z. Chen, *Nanoscale*, 2012, **4**, 2590-2596.

41 H. Sun, K. Xu, M. Huang, Y. Shang, P. She, S. Yin and Z. Liu, *Appl. Surf. Sci.*, 2015, **357**, 69-73.

42 S. W. Chang Chien, H. L. Chen, M. C. Wang and K. Seshaiah, *Chemosphere*, 2009, **74**, 1125-1133.

43 T. Gao, P. Norby, F. Krumeich, H. Okamoto, R. Nesper and H. Fjellvag, *J Phys Chem C*, 2010, **114**, 922-928.

44 A. Ramírez, P. Hillebrand, D. Stellmach, M. M. May, P. Bogdanoff and S. Fiechter, *J.Phys. Chem. C*, 2014, **118**, 14073-14081.
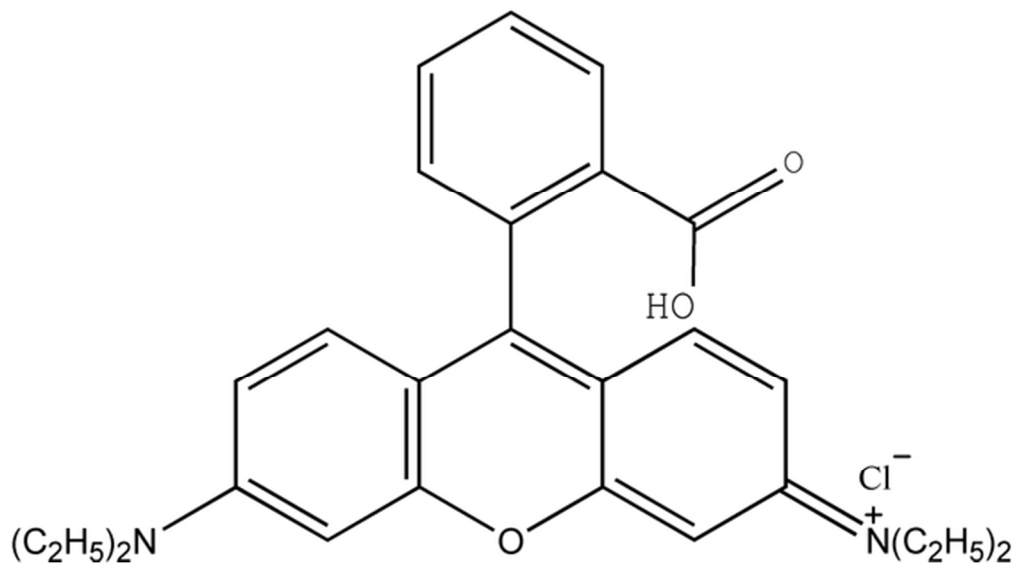
Scheme. 1 Molecular model of Rhodamine B
55x30mm (300 x 300 DPI)
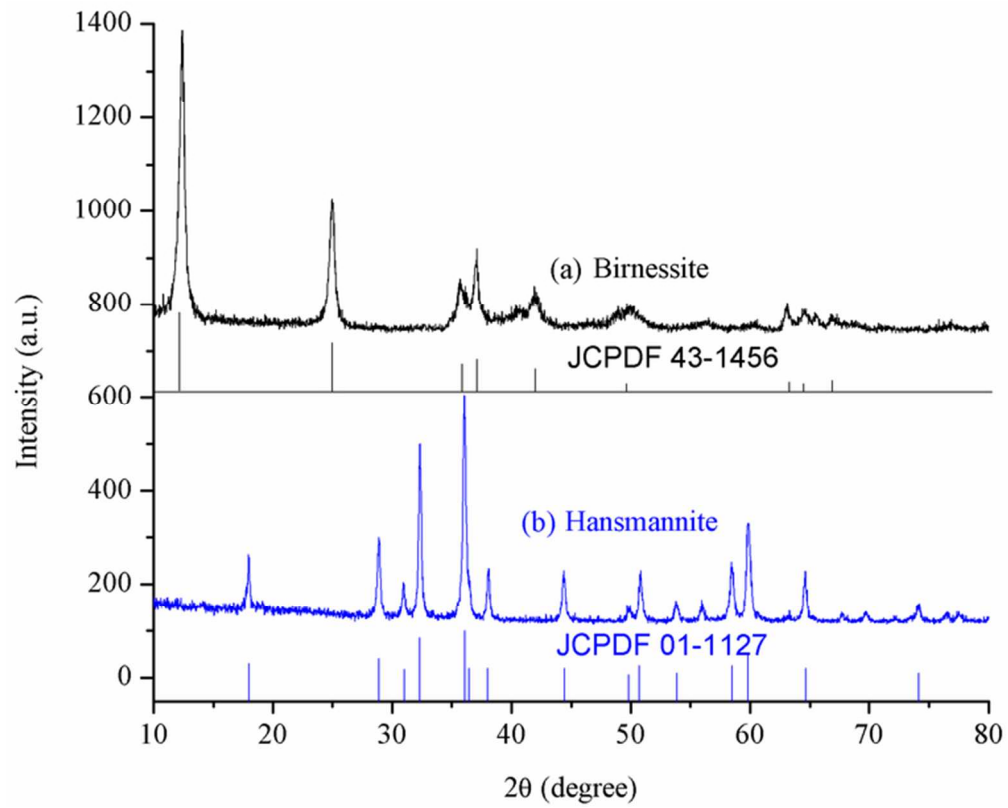
Fig.1. XRD pattern of the synthesized products: (a) with EDTA-Na, (b) without EDTA-Na.
64x51mm (300 x 300 DPI)
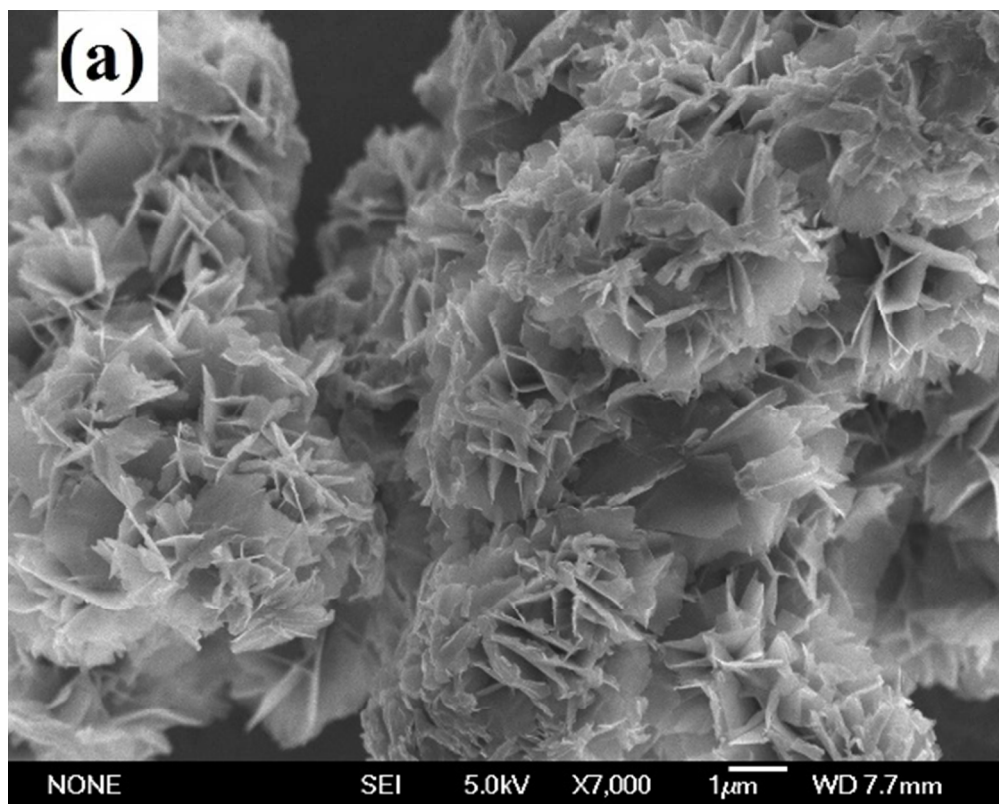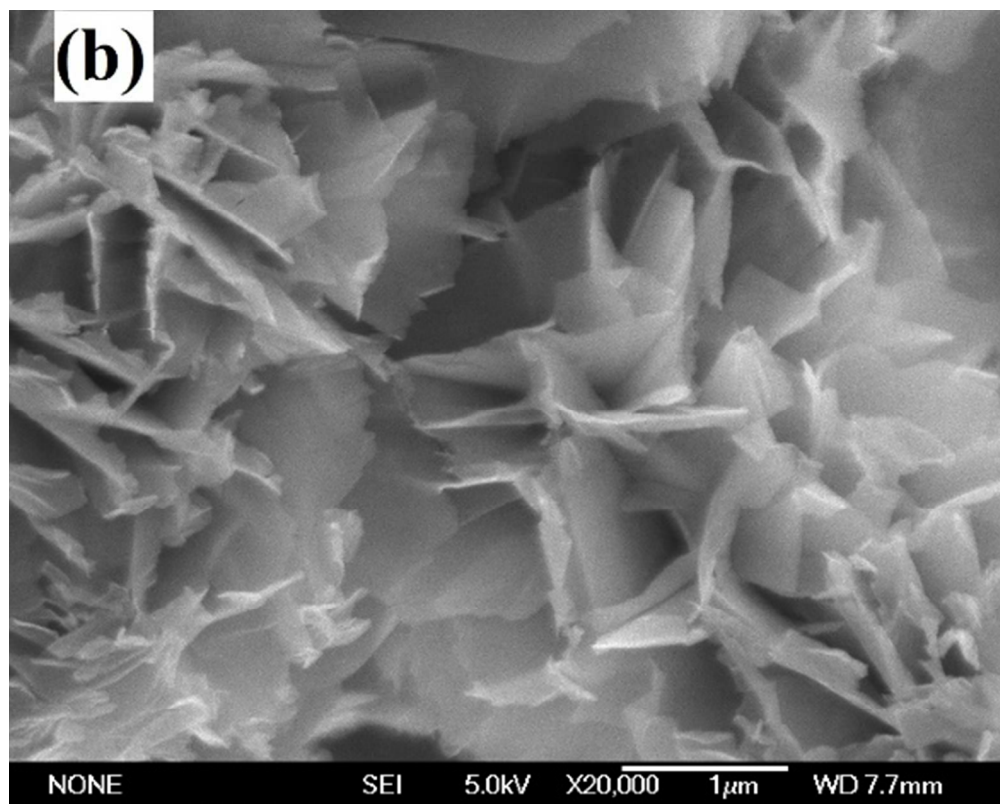
68x54mm (220 x 220 DPI)

67x54mm (220 x 220 DPI)
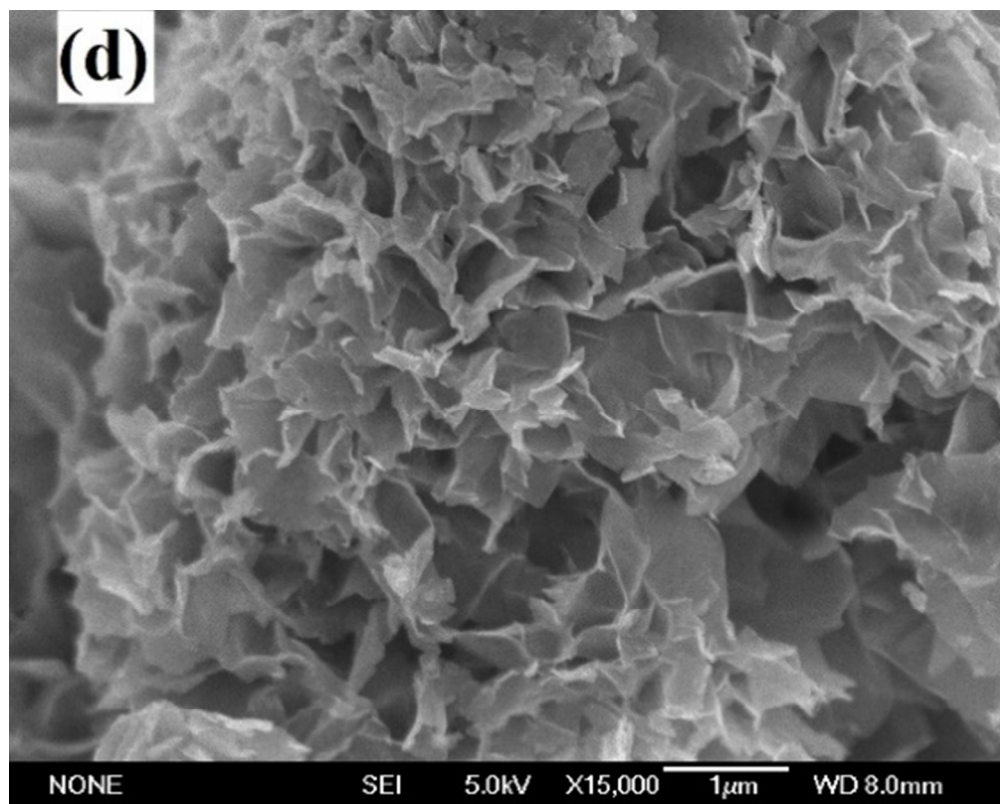
NONE   SEI   5.0kV   X6,500   1μm   WD 8.0mm

68x54mm (220 x 220 DPI)

Fig. 2 Typical SEM images of birnessites prepared under the molar ratio of MnSO$_4$/EDTA-Na equals to 1 (a), (b) and the ratio equals to 2 (c), (d). The lower-magnification image are shown in (a), (c), while the higher-magnification images are presented in (b), (d).
68x54mm (220 x 220 DPI)
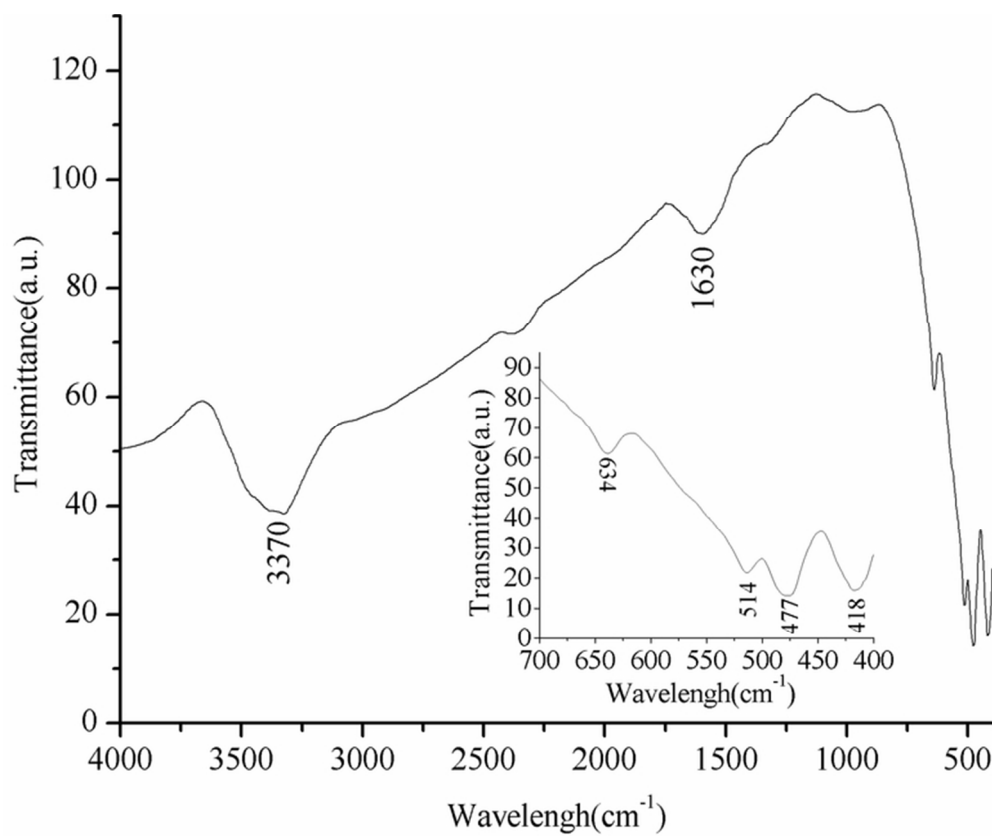
Fig. 3. FTIR spectra of birnessite, the inset shows partially enlarged spectra in the range of 700−400 cm^{-1}.
65x54mm (300 x 300 DPI)
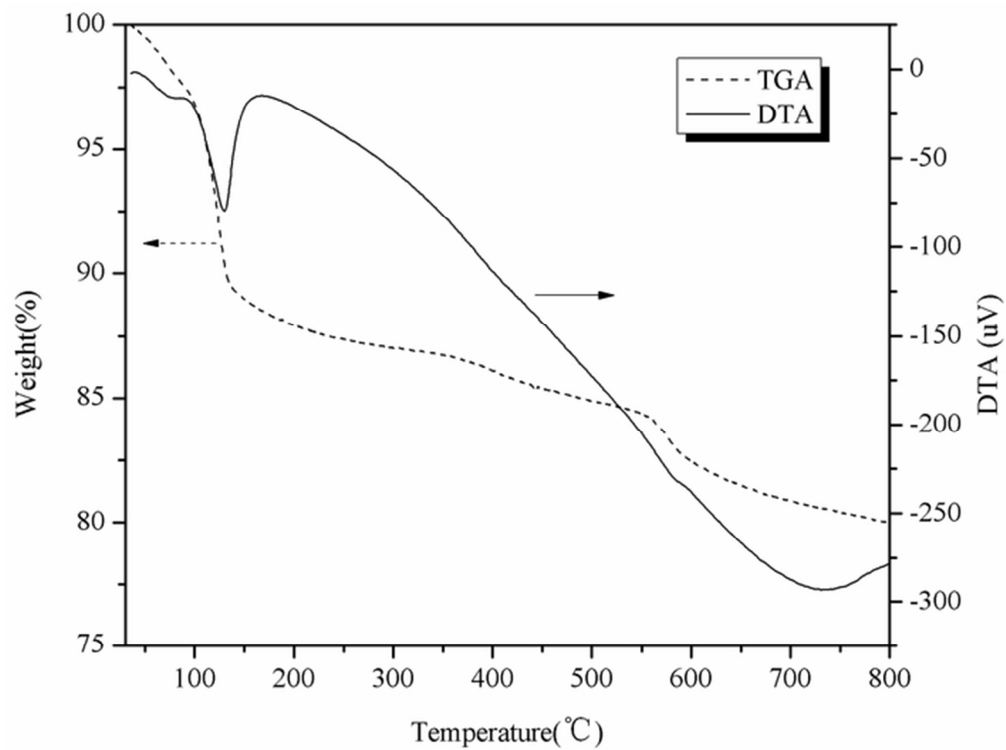
Figure 4. TG-DTA curves of birnessite in N$_2$. Heating rate: 10 °C/min.
59x44mm (300 x 300 DPI)
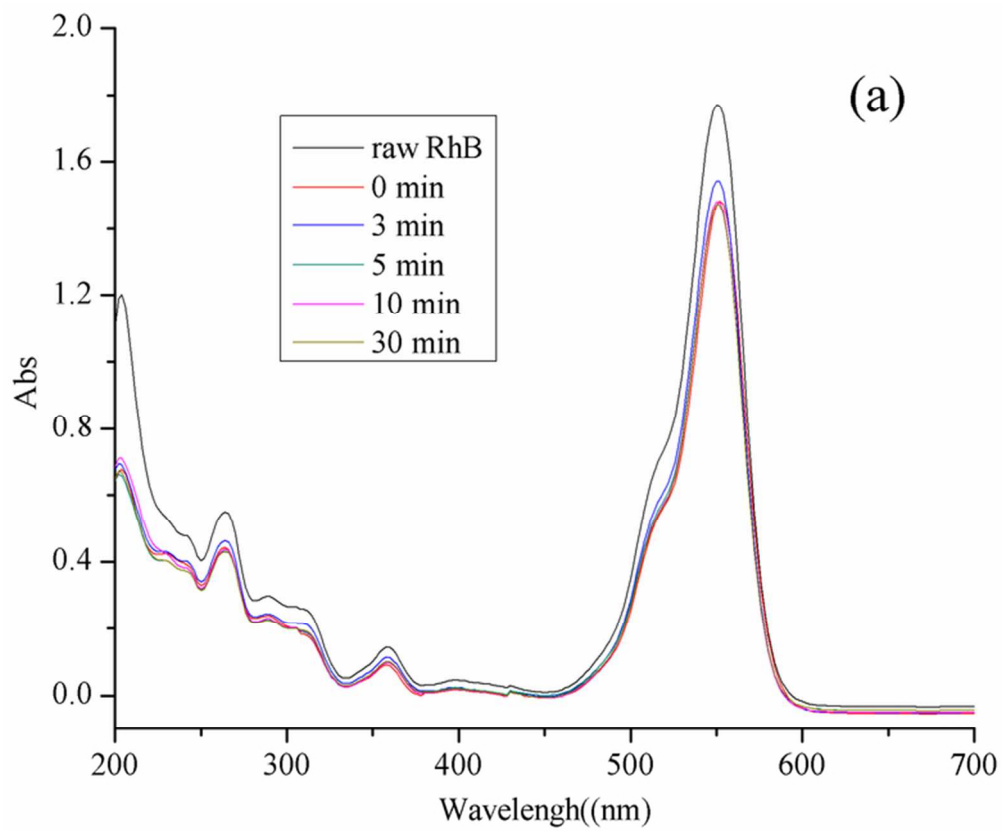
65x54mm (300 x 300 DPI)
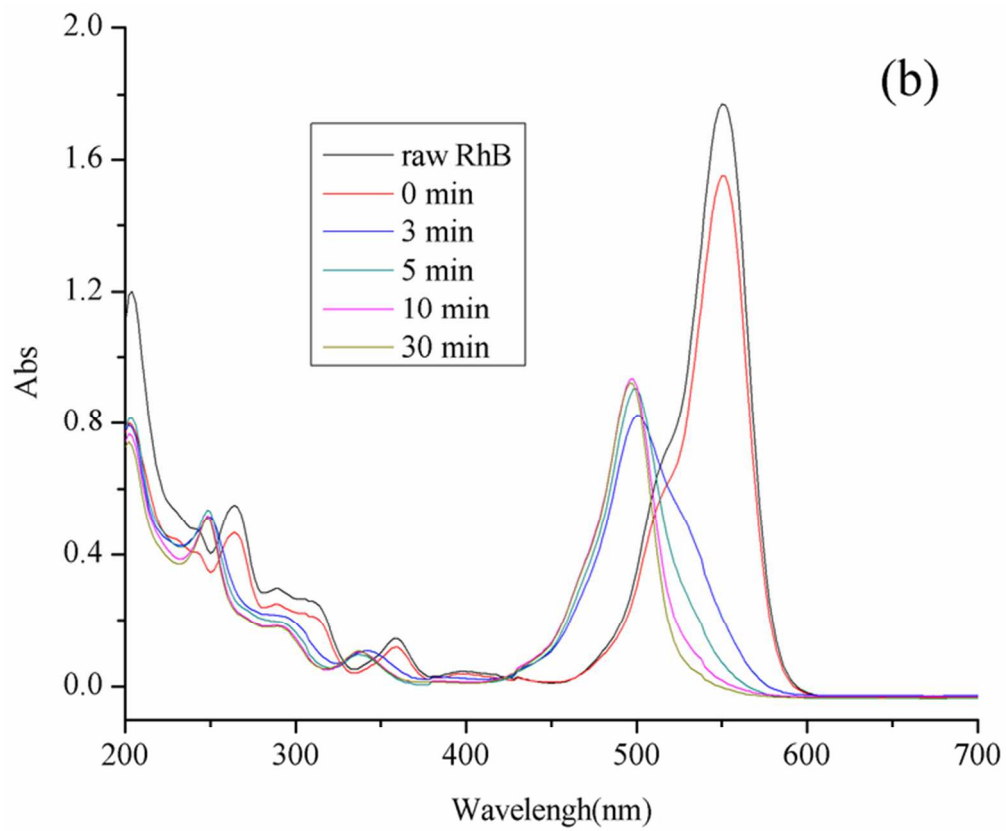
66x54mm (300 x 300 DPI)
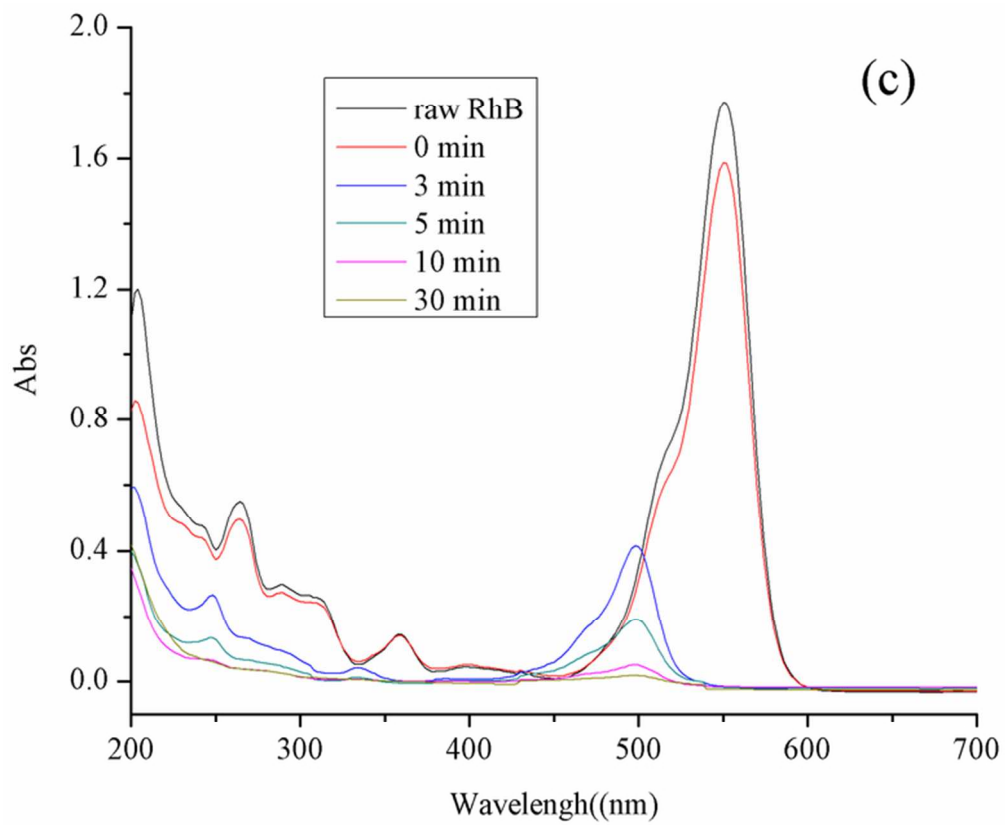
65x53mm (300 x 300 DPI)
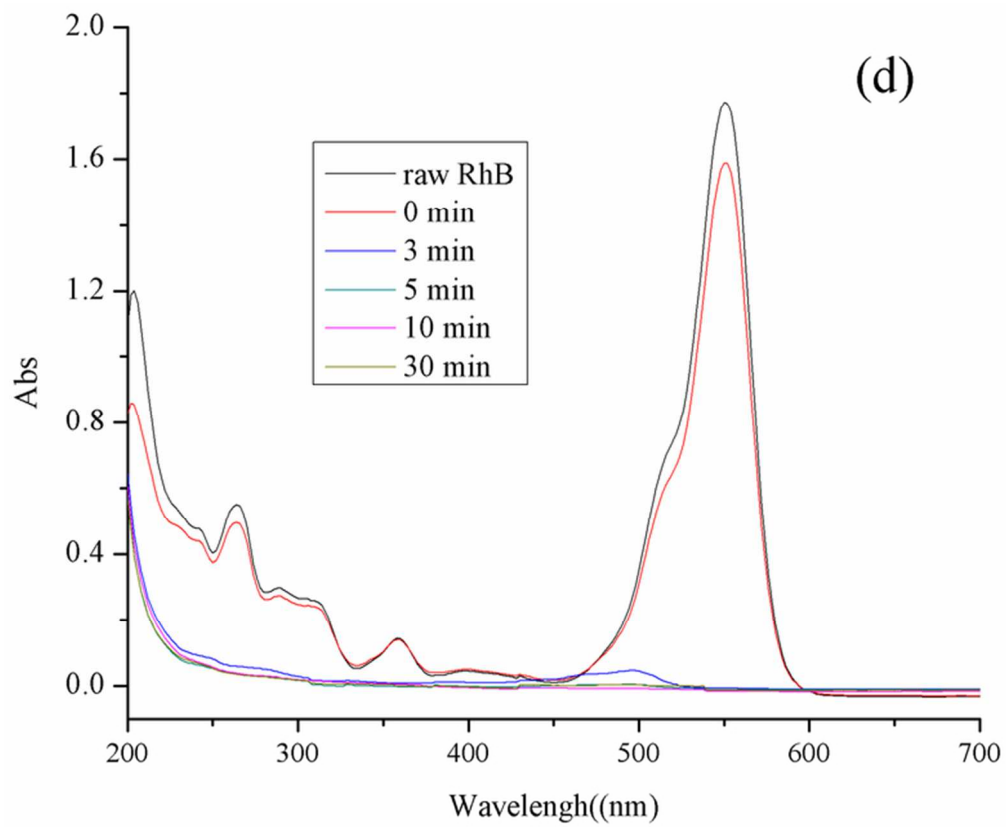
65x54mm (300 x 300 DPI)
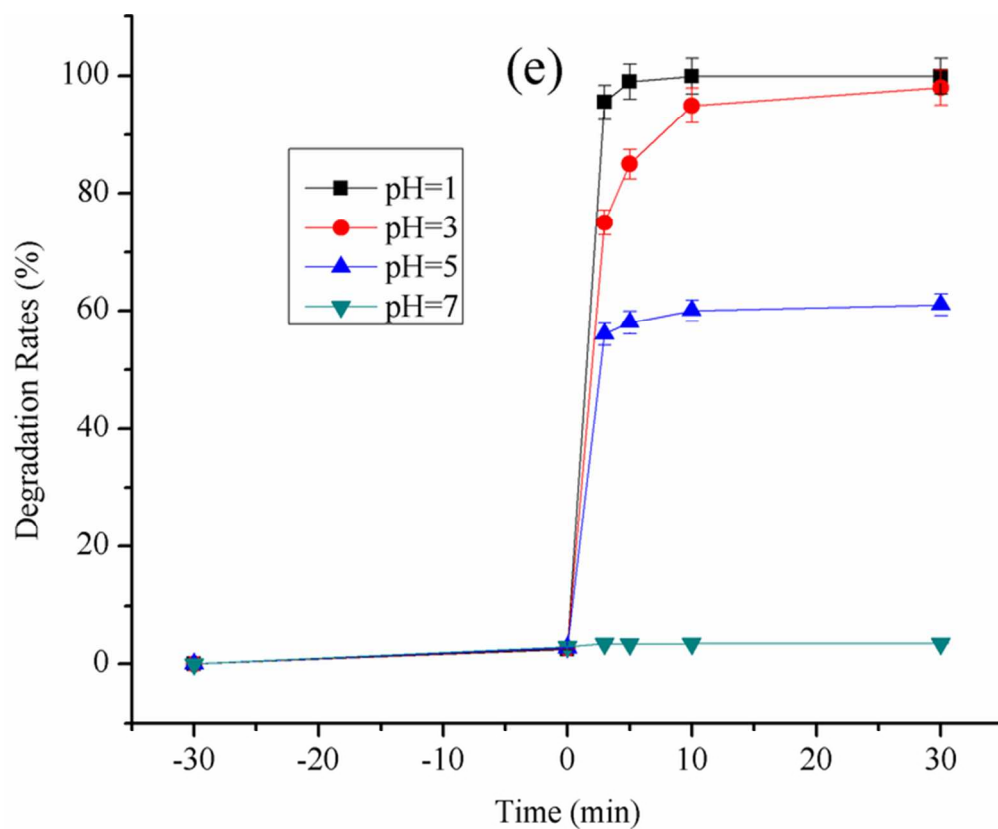
Fig. 5. The UV-vis spectra of RhB during degradation under different pH: (a) pH=7; (b) pH=5; (c) pH=3; (d) pH=1. (e) Detailed degradation rates under different pH values.
65x53mm (300 x 300 DPI)
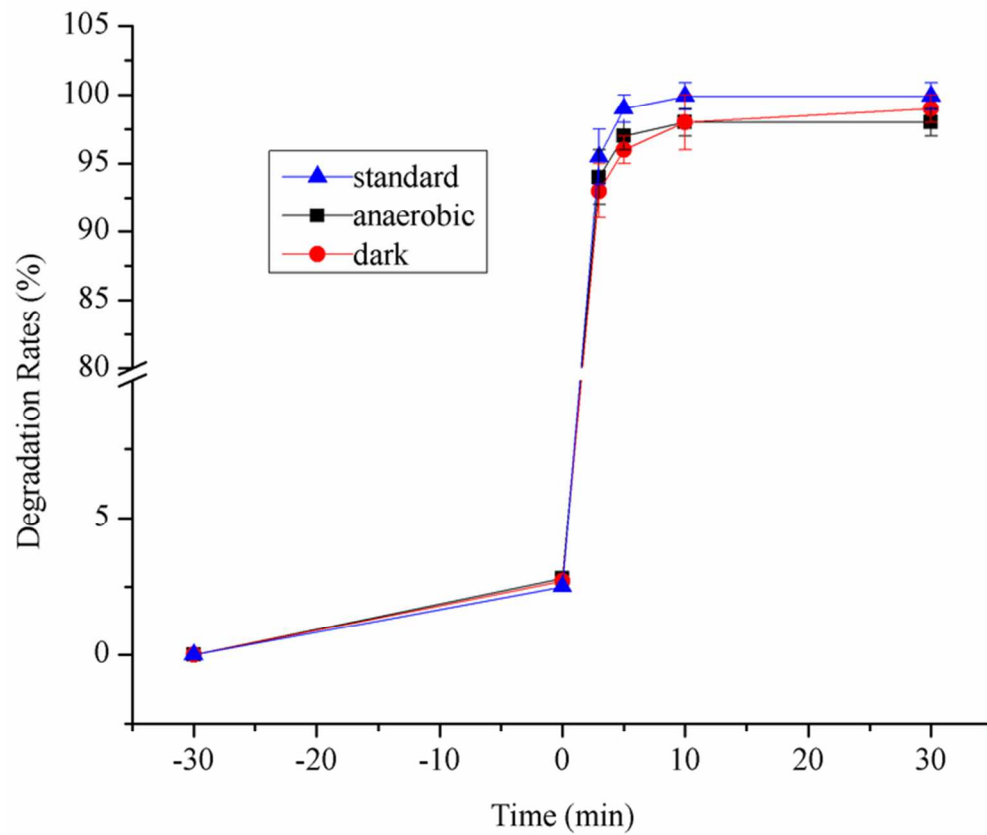
Fig. 6. The degradation rates of RhB under different experimental conditions
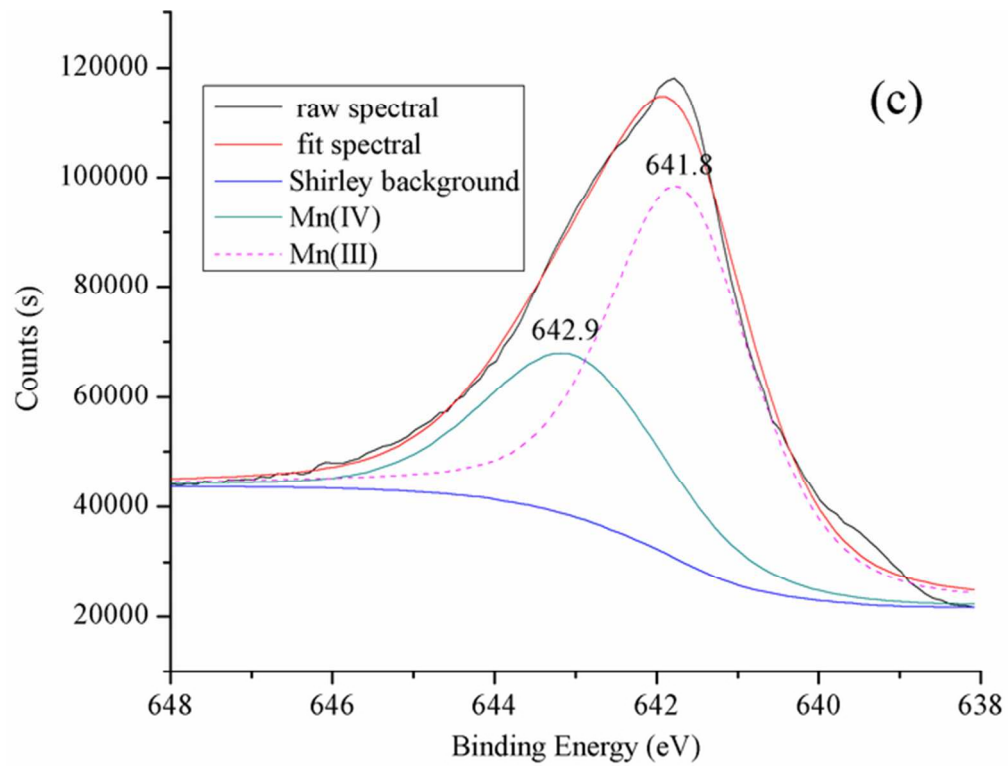66x55mm (300 x 300 DPI)
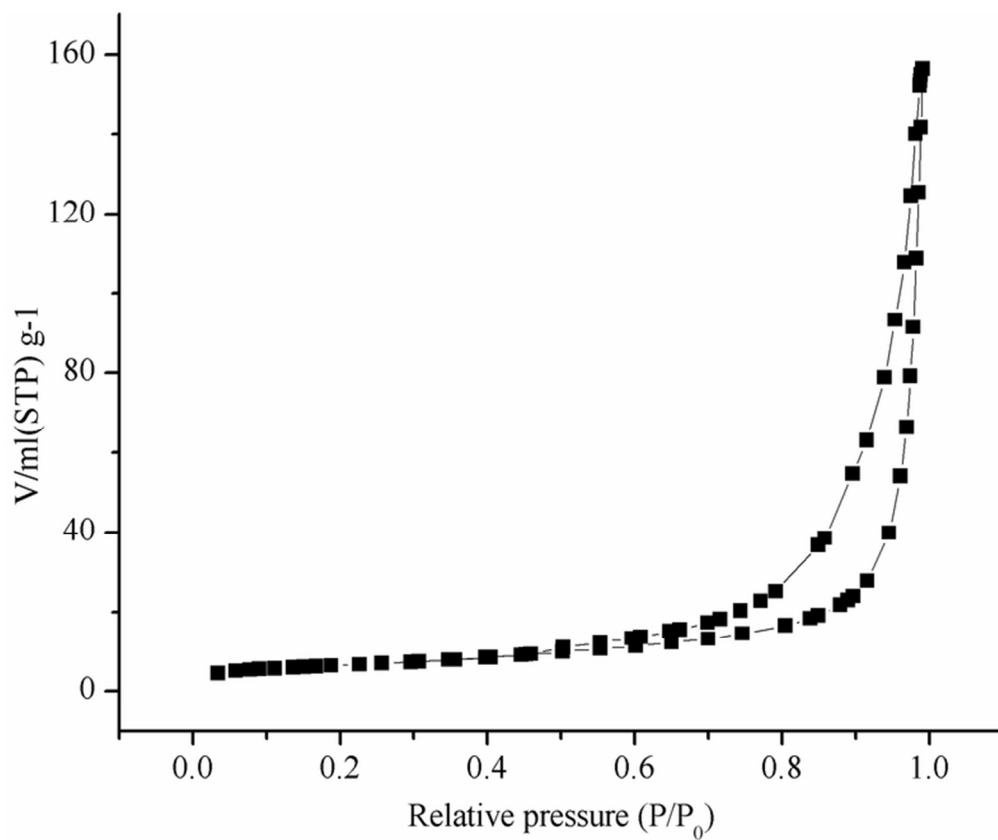
Fig. 7. N_2 adsorption–desorption isotherms of birnessite
66x55mm (300 x 300 DPI)
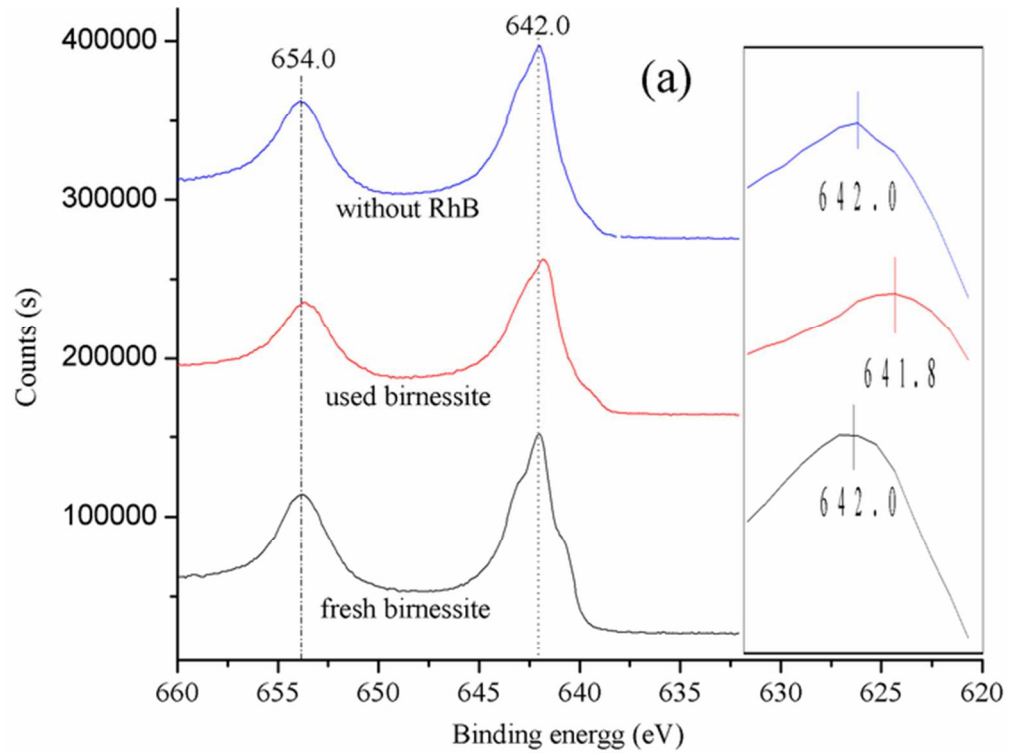
59x44mm (300 x 300 DPI)
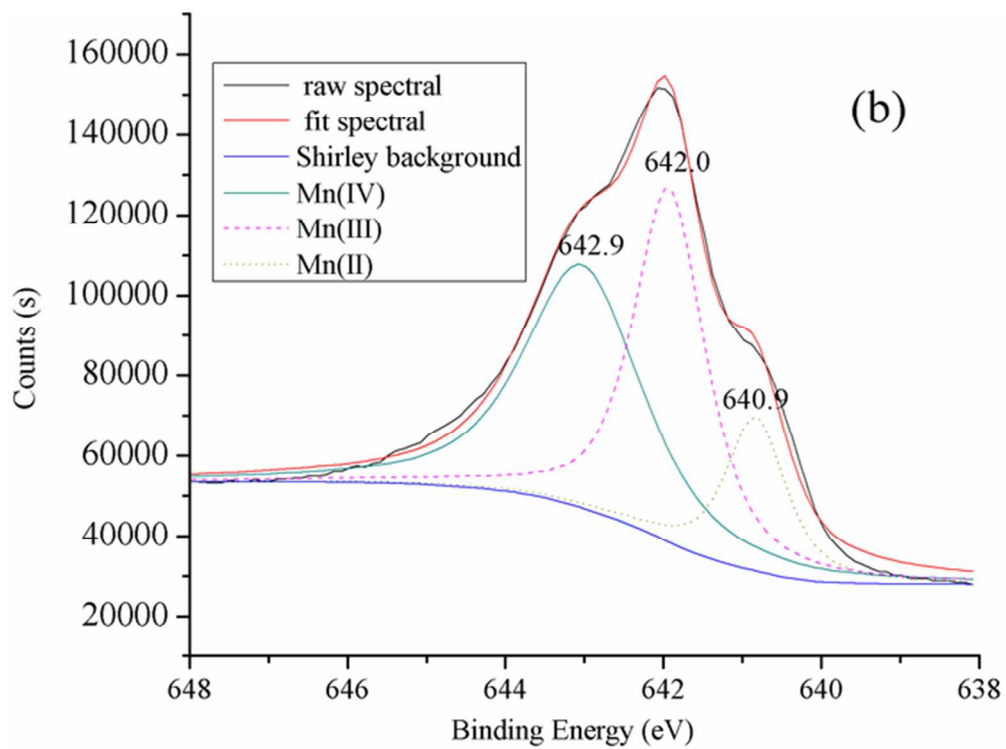
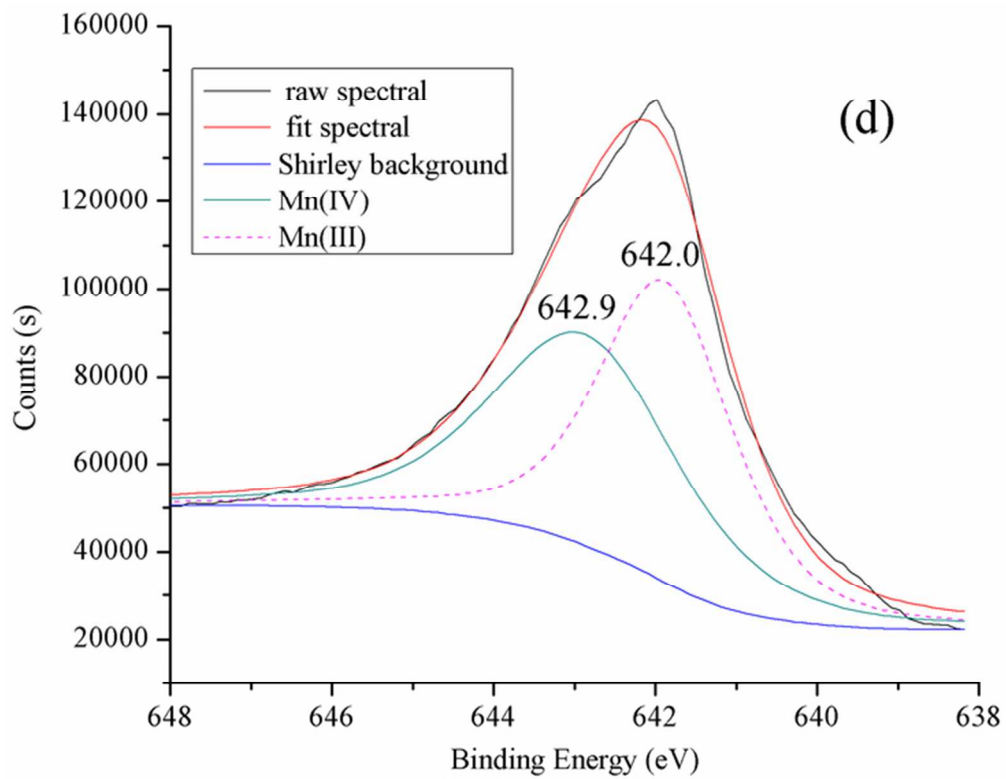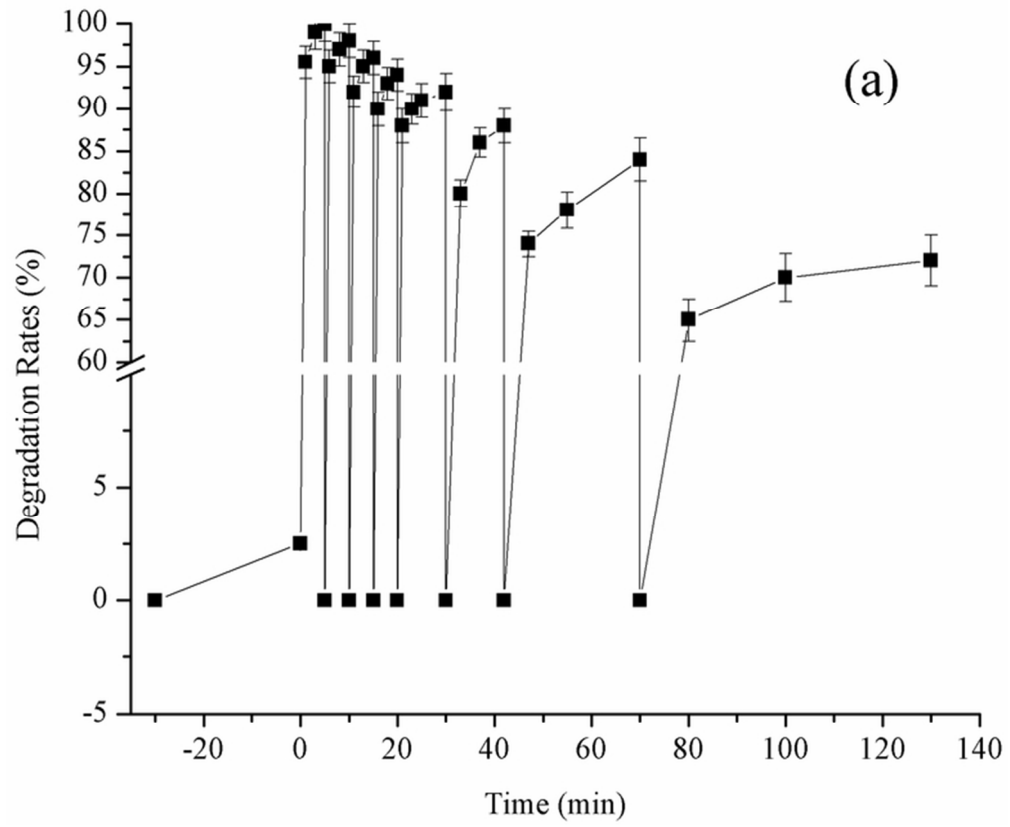58x43mm (300 x 300 DPI)

60x45mm (300 x 300 DPI)

Fig. 8. XPS spectra of fresh birnessite, used birnessite and birnessite treated in acid solution without RhB: (a) Mn2p, insert was the Mn2p XPS around 642 eV. Mn (2p$_{3/2}$) for those samples respectively: (b), (c) and (d).
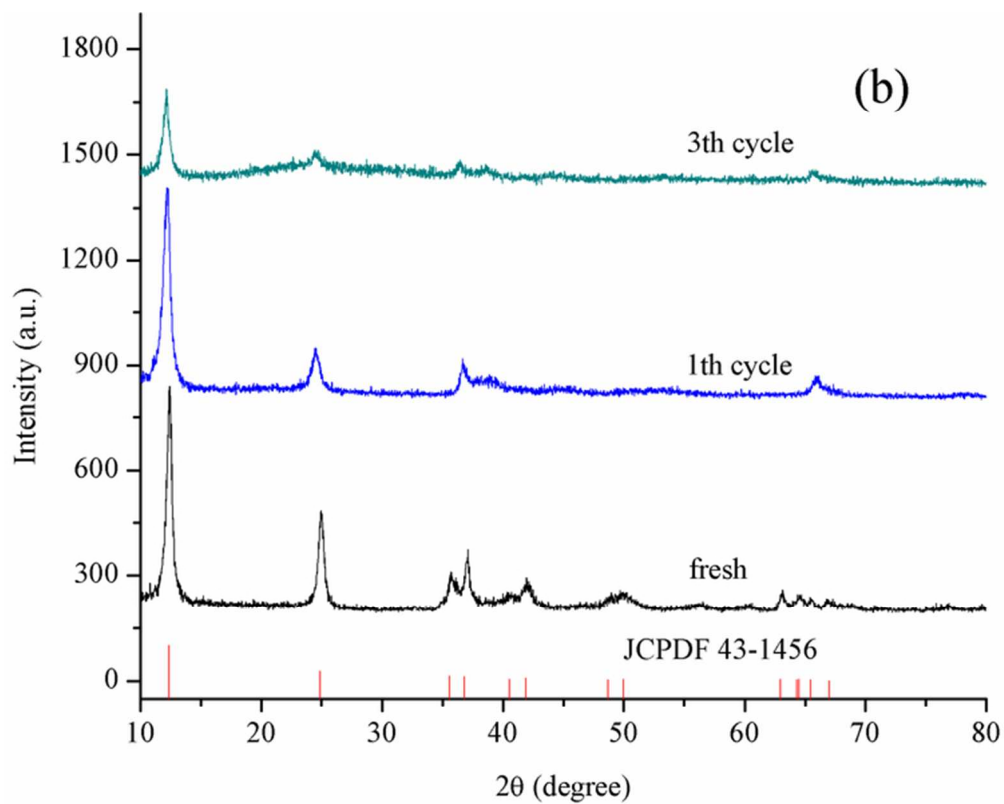61x48mm (300 x 300 DPI)

65x54mm (300 x 300 DPI)

Fig. 9. (a) Degradation rates of RhB in a consecutive batch, (b) XRD patterns of sample after several cycles.
63x50mm (300 x 300 DPI)

A facile synthesis of high purity microflower birnessite and its efficient oxidative degradation of RhB